SCIENCE CHINA
Information Sciences

• RESEARCH PAPER •

November 2023, Vol. 66 212302:1–212302:13
https://doi.org/10.1007/s11432-022-3709-y

Randomly coupled trench-assisted multicore fibers with different arrangements for high tolerance of manufacturing errors

Yongneng JIANG[1], Jiajing TU[1*], Shecheng GAO[1], Weiping LIU[1] & Zhaohui LI[2,3]

[1]*Department of Electronic Engineering, College of Information Science and Technology, Jinan University, Guangzhou* 510632*, China;*
[2]*School of Electronics and Information Technology, Guangdong Provincial Key Laboratory of Optoelectronic Information Processing Chips and Systems, Sun Yat-sen University, Guangzhou* 510006*, China;*
[3]*Southern Marine Science and Engineering Guangdong Laboratory (Zhuhai), Zhuhai* 519082*, China*

Received 31 October 2022/Revised 20 January 2023/Accepted 16 February 2023/Published online 7 October 2023

Abstract Randomly coupled multicore fibers (RC-MCFs) are promising candidates for long-haul transmission. However, the degree of coupling between the homogeneous cores of an RC-MCF is weakened if manufacturing errors appear. Therefore, a low-index trench layer is introduced into the coupled cores to investigate the effects of its position and thickness on the group index to enhance the tolerance of manufacturing errors. A depressed region is designed in the center of the core to solve the problem of the effective area decreasing because of the confinement of the low-index trench. Additionally, it is important to study the effective arrangement of the coupled cores to obtain a smaller group delay spread (GDS) within the limited 125-μm cladding; we discuss the single-layer and double-layer arrangements. A moderate range is found for both the bending radius and core pitch to minimize the GDS. For the single-layer arrangement, the degree of mixing is weak, and the degeneracy state does not easily change the bending conditions; thus, it may be a good candidate for designing systemically coupled multicore fibers. For the double-layer arrangement, the bending and twisting factors can induce sufficient mixing among the different modes to reduce GDS; thus, this arrangement is more suitable for the design of RC-MCFs.

Keywords manufacturing errors, randomly coupled multicore fibers, trench-assisted core, single-layer arrangement, double-layer arrangement

Citation Jiang Y N, Tu J J, Gao S C, et al. Randomly coupled trench-assisted multicore fibers with different arrangements for high tolerance of manufacturing errors. Sci China Inf Sci, 2023, 66(11): 212302, https://doi.org/10.1007/s11432-022-3709-y

1 Introduction

Space-division multiplexing (SDM) has been proposed to increase the transmission capacity of fiber transmission systems [1, 2] and overcome the capacity limitation of conventional single-mode fibers (SMFs), which is approximately 100 Tb/s [3, 4]. A multicore fiber (MCF), an SDM technology, transmits multiple different signals simultaneously by providing multiple spatial channels in the cladding such that the transmission capacity increases accordingly [5, 6]. Furthermore, MCFs can be classified into weakly coupled MCFs (WC-MCFs) and strongly coupled MCFs (SC-MCFs) based on the degree of coupling between adjacent cores [7, 8].

WC-MCFs have a sufficiently large core pitch (Λ) to reduce the crosstalk (XT) among the neighboring cores, and thus, each core can be regarded as an independent waveguide [9, 10]. By comparison, SC-MCFs have a smaller Λ and make the inter-core XT nonnegligible, which requires multi-input multi-output digital-signal-processing (MIMO-DSP) algorithms for XT compensation [11, 12]. When the Λ of the SC-MCF is very small, the eigenmodes propagating in the fiber are distributed as orthogonal and uncoupled modes on all cores, which are the so-called "supermodes" [13, 14]. The effective index (n_{eff})

* Corresponding author (email: tujiajing@jnu.edu.cn)

of the supermodes of each order maintains a large difference, and thus, they can propagate stably and independently without energy mixing, which corresponds to the "adiabatic" state [15]. In this case, all strongly coupled cores can be regarded as a composite large core, and multiple supermodes are propagated in this equivalent core [16], which is similar to a few-mode fiber [17–20]. This is described as a "strongly coupled, weakly mixed" state, and this type of SC-MCF is called a systematically coupled MCF [21], in which the width of the impulse response increases linearly with the transmission distance (L). When Λ is moderate, a strongly coupled state emerges among the cores, and the n_{eff} difference (Δn_{eff}) among the supermodes of each order decreases (ideally, the Δn_{eff} among the supermodes decreases with the increase in Λ [16]). Therefore, random mixing occurs when the supermode propagates along a fiber disturbed by external perturbations, such as bending and twisting. This is described as a "strongly coupled, strongly mixed" state, and this type of SC-MCF is called a randomly coupled MCF (RC-MCF), which can enable the width of the impulse response to be proportional to the square root of L [22–25]. There is a large amount of energy mixing among the cores of RC-MCFs, such that light launched into a specific core is evenly distributed in all cores after a short L; thus, the mode-dependent loss (MDL) can be reduced [26–28]. Features, such as low group delay spread (GDS), low MDL, and large effective area (A_{eff}) (low nonlinearity [29–31]), make RC-MCFs promising candidates for next-generation ultra-large-capacity and ultra-long-distance communications.

In this study, we focus on the design and analysis of an RC-MCF. It should be noted that the degree of coupling among the cores in the RC-MCF is weakened if the homogenous cores have manufacturing errors. Therefore, intensifying manufacturing error tolerance is key in the design of RC-MCFs. A trench-assisted (TA) core, which not only achieves a higher spatial density but also regulates the group index (n_{g}) of the core to enhance the tolerance of manufacturing errors, was proposed in [32]. However, the influence of the trench position on n_{g} has not been explored, and the reduction in A_{eff} caused by the addition of a trench has not been solved. Meanwhile, RC-MCFs can accommodate a maximum of 12 cores at a standard cladding diameter of 125 μm [33], but the issue of how to efficiently arrange strongly coupled cores to obtain smaller GDS has not yet been investigated. In this study, we adopt a TA-core with a depressed region inside the center and discuss the regulation of the trench thickness and position on the n_{g} while ensuring that its A_{eff} is larger than 80 μm^2. This is then employed as a subcomponent of a 12-core RC-MCF, and a randomly coupled trench-assisted MCF (RC-TA-MCF) is formed. The degree of mixing and dependence of GDS on the Λ and bending radius (R_{b}) for the RC-TA-MCF under different arrangements are also discussed.

2 Design of core profile and arrangement

2.1 Core profile and regulation of the group index

Owing to unavoidable manufacturing errors [34], the parameters of fabricated cores differ from those of designed homogeneous cores. Therefore, a low-index trench layer is introduced to regulate n_{g}, thus improving the tolerance to manufacturing errors [32]. n_{g} is defined as [32, 35]

$$n_{\text{g}} = c\frac{\mathrm{d}\beta}{\mathrm{d}\omega}, \tag{1}$$

where c is the speed of light in vacuum, β is the propagation constant, and ω is the angular frequency of the light wave.

We adopt a TA-core as shown in Figure 1(a) to design the RC-TA-MCF, where a denotes the radius of the inner core, r_1 denotes the radius of the high-index core, r_2 denotes the distance from the center of the core to the inner edge of the trench layer, r_3 denotes the distance from the center of the core to the outer edge of the trench layer, W denotes the width of the trench layer, Δ_1 denotes the relative index difference between the high-index core and the cladding, Δ_2 denotes the relative index difference between the inner core and the cladding, and Δ_{tr} denotes the relative index difference between the trench layer and the cladding. It supports only the fundamental mode, including two degenerated linearly polarized modes. Compared with the conventional single-mode step index fiber (SIF) ($\Delta = (n_{\text{co}} - n_{\text{cl}})/n_{\text{co}} = 0.35\%$, $r_1 = 4.5$ μm, $A_{\text{eff}} = 82$ μm^2, and $n_{\text{cl}} = 1.444$ at $\lambda = 1550$ nm), the low-index trench layer reduces the A_{eff} of the core mode. Therefore, based on the structure in [32], an inner depressed core is added to increase A_{eff}. The dependence of the inner core parameters (Δ_2 and a) on A_{eff} is shown in Figure 1(b),

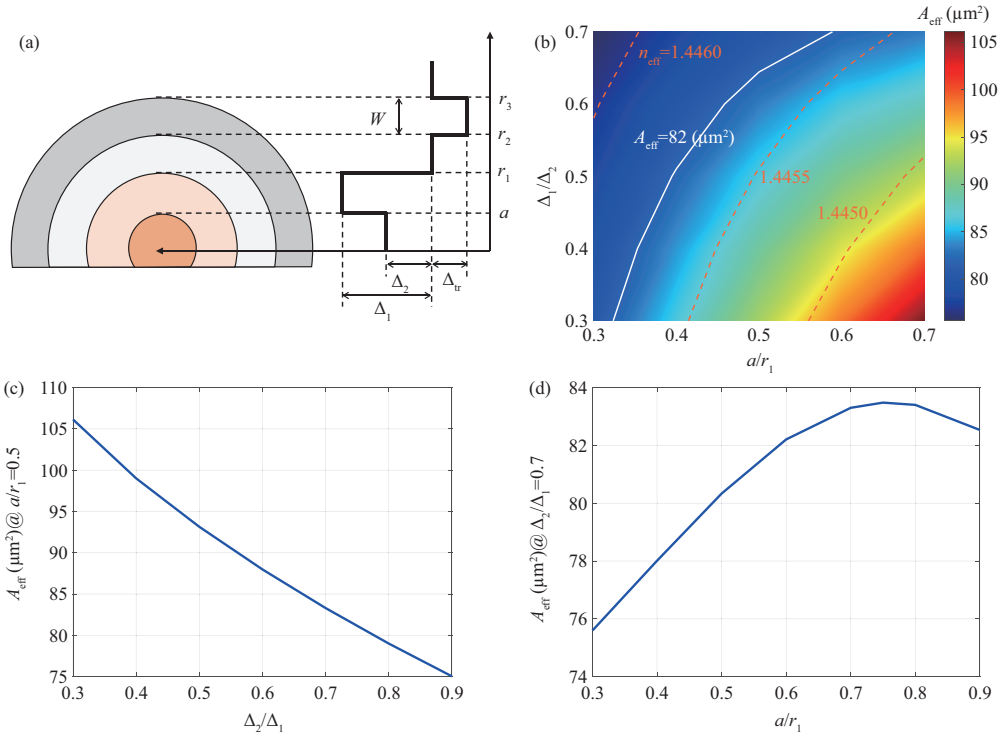

Figure 1 Design of the TA-core. (a) Schematic of index profile of TA-core, (b) dependence of A_{eff} on inner core parameters (Δ_2 and a), (c) dependence of A_{eff} on Δ_2/Δ_1 when $a/r_1 = 0.5$, and (d) dependence of A_{eff} on a/r_1 when $\Delta_2/\Delta_1 = 0.7$.

where $r_1 = 4.5$ μm, $\Delta_1 = 0.35\%$, $\Delta_{\text{tr}} = -0.7\%$, $r_2/r_1 = 1.5$, and $W/r_1 = 0.32$. In Figure 1(b), the background color indicates A_{eff}, the solid white line represents $A_{\text{eff}} = 82$ μm^2, which equals the A_{eff} of a conventional single-mode SIF, and the orange dashed line represents the n_{eff} of the core-mode. The vertical line with $a/r_1 = 0.5$ in Figure 1(b) is plotted separately to obtain Figure 1(c), and the horizontal line with $\Delta_2/\Delta_1 = 0.7$ in Figure 1(b) is plotted separately to obtain Figure 1(d). As shown in Figure 1(c), A_{eff} decreases as Δ_2 increases when a is fixed (still keeping the single-mode condition). In addition, from Figure 1(d), when Δ_2 is larger and fixed, A_{eff} first increases with increasing a and then gradually converges or possibly decreases. To better utilize the inner core to increase A_{eff}, a should not be larger. Because the supermode is a linear superposition of the mode field of each core [13, 14], to maintain a larger A_{eff} for each core, the parameters of the inner core are set as $a = r_1/2$ and $\Delta_2 = \Delta_1/2$.

A fabricated core with manufacturing errors has size r_e that may have either a positive or negative offset relative to the originally designed core size r_o. x is the relative core size difference between the fabricated core and originally designed core, where $x = (r_e - r_o)/r_o$. Thus, the range of the maximum relative size difference of the fabricated cores is between $-x$ and $+x$. Here, we define the n_{g} difference among two TA-cores ($n_{\text{g1}} - n_{\text{g2}}$) as ΔNg, where n_{g1} and n_{g2} correspond to the core group index of the positive and negative core size offset, respectively. To understand the regulation effect of the TA-core shown in Figure 1(a) on ΔNg caused by manufacturing errors, we assume that the core manufacturing errors are reflected in the core radius as $r_1 \pm 1\%$, $r_1 \pm 2\%$, and $r_1 \pm 5\%$, respectively. Figure 2 shows the dependence of ΔNg on the relative trench width W/r_1 for different values of r_2/r_1, where $r_1 = 4.5$ μm, $a = r_1/2$, $\Delta_1 = 0.35\%$, $\Delta_2 = \Delta_1/2$, $\Delta_{\text{tr}} = -0.7\%$, and $r_3 = r_2 + W$. As shown in Figure 2, even if the core size error is reduced to $r_1 \pm 1\%$, the ΔNg of the core without trench assistance ($W/r_1 = 0$) is in the order of 10^{-5}, which is comparable to Δn_{eff} between adjacent orders of supermodes. It can also be confirmed that it is not only W that has a regulating effect on ΔNg, but also the position of the trench layer. When r_2/r_1 is small, ΔNg first increases and even exceeds the value of ΔNg without introducing the trench layer, and then decreases with the increase of W/r_1, as shown in Figure 2(a). With the increase in r_2/r_1, the zero value point of ΔNg also fluctuates with the value of W/r_1. After reaching a certain larger value of r_2/r_1, ΔNg tends to stabilize, and the zero value point also disappears, as shown in Figures 2(b)–(d). This is because the trench layer moves away from the core with the increase in r_2/r_1, which weakens confinement and regulation; however, regulation persists. It should be noted that ΔNg does not always

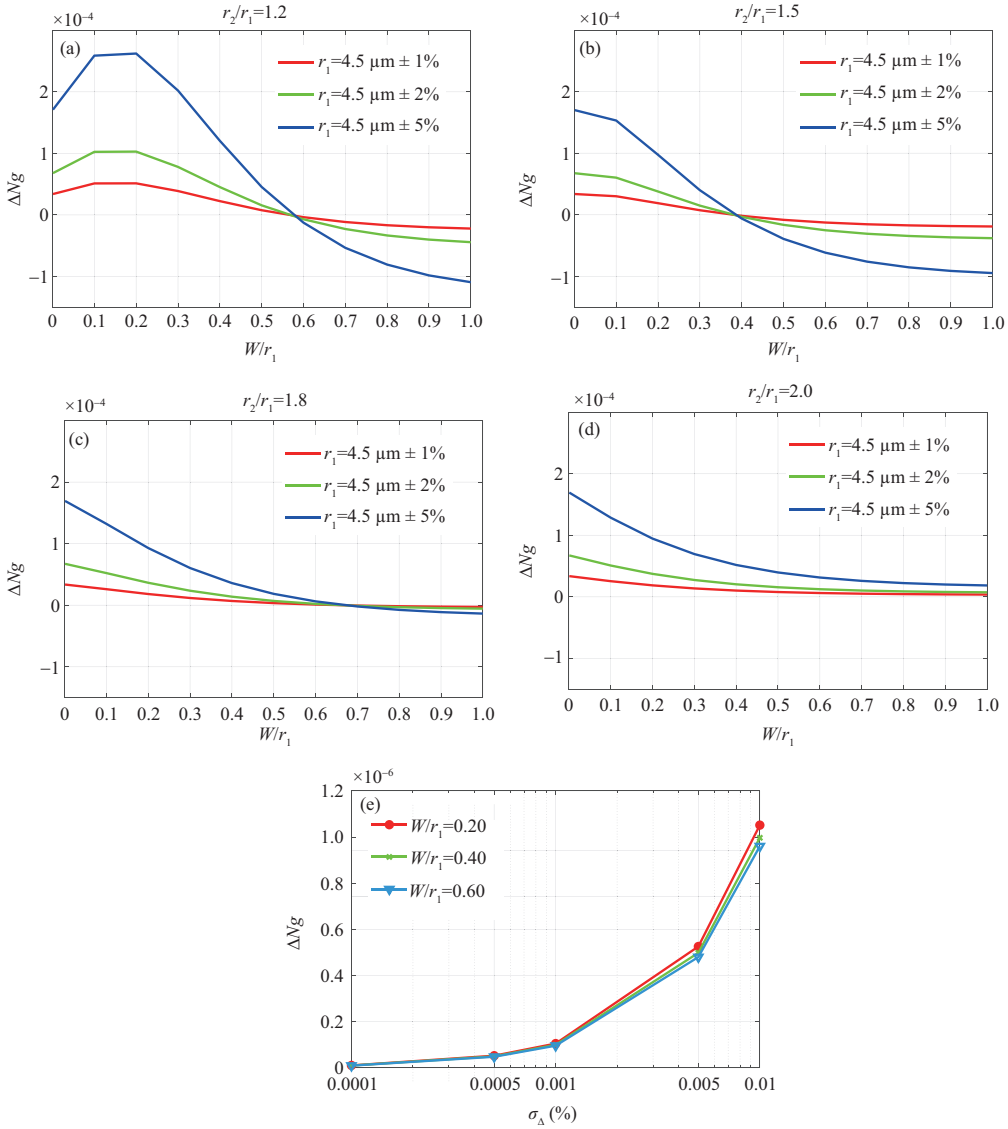

Figure 2 Dependence of ΔNg on the W/r_1 for different values of r_2/r_1, (a) $r_2/r_1 = 1.2$, (b) $r_2/r_1 = 1.5$, (c) $r_2/r_1 = 1.8$, and (d) $r_2/r_1 = 2.0$; (e) dependence of ΔNg on the σ_Δ for different values of W/r_1.

decrease with the increase in W and it becomes zero at approximately a certain W/r_1 value. We then consider the effect of index error on $\Delta N\mathrm{g} = n_{\mathrm{g}1} - n_{\mathrm{g}2}$, where $n_{\mathrm{g}1}$ and $n_{\mathrm{g}2}$ denote the group index of the cores with positive (+) and negative (−) index errors, respectively. The parameters are set as follows: $r_1 = 4.5$ μm, $a = r_1/2$, $r_2/r_1 = 1.5$, $\Delta_1 = 0.35\% \pm \sigma_\Delta$, $\Delta_2 = \Delta_1/2$, $\Delta_{\mathrm{tr}} = -0.7\% \pm \sigma_\Delta$, and $\lambda = 1550$ nm, where σ_Δ represents the variation of the relative index difference due to manufacturing errors; the results are shown in Figure 2(e). We can reasonably assume that σ_Δ is 0.001% [35]; at this time, the magnitude of ΔNg is 10^{-7} and hardly varies with W/r_1. As the magnitude of ΔNg variation caused by σ_Δ is much smaller than that caused by the geometric size, in our subsequent discussion, the manufacturing errors are all mapped to the size variations. Thereafter, for the convenience of discussion, the parameters of the core structure are adopted as $r_1 = 4.5$ μm, $a = r_1/2$, $\Delta_1 = 0.35\%$, $\Delta_2 = \Delta_1/2$, $\Delta_{\mathrm{tr}} = -0.7\%$, $r_2/r_1 = 1.5$, and $W/r_1 = 0.38$, which correspond to $A_{\mathrm{eff}} = 85$ μm^2 at $\lambda = 1550$ nm.

2.2 Core arrangement and degree of mixing

The degree of coupling of an MCF with fixed structural parameters is mainly determined by its Λ, and thus, the types and characteristics of MCFs can be summarized from the perspective of Λ (degree of coupling), as shown in Table 1 [15, 21]. In MCFs with too small or too large Λ, strong mixing among the supermodes cannot be obtained [11, 16] because the larger coupling coefficients and smaller Δn_{eff}

Table 1 Summary of types and characteristics of MCF

Fiber type	Strongly coupled MCF		Weakly coupled MCF
	Systematically coupled MCF	Randomly coupled MCF	
Core pitch Λ	Small	Medium	Large
Coupling process	Adiabatic & systematical	Nonadiabatic & random	Nonadiabatic
Power transfer	Negligible	Uniform distribution	Power fully transfers at phase matching point
State	Strongly coupled & weakly mixed	Strongly coupled & strongly mixed	Weakly coupled
MIMO configuration	High complexity	High complexity	Low complexity
Growth of GDS to transmission distance & dominant factor	ps/km (linear) & supermode DMD	ps/$\sqrt{\text{km}}$ (square root)	ps/km (linear) & manufacturing errors induced inter-core skew
The mode coupling between cores is strong and systematic (deterministic), and thus the term "systematically coupled" is used in [21]			

between the adjacent modes are necessary conditions to maintain the strongly mixed state in RC-MCFs. As Λ decreases, the coupling coefficient becomes larger due to the higher spatial overlap of the mode fields. However, as Λ decreases, Δn_{eff} becomes larger due to the formation of stable supermodes. Only when Λ is moderate, can there be large energy mixing among the cores of the RC-MCF, such that the power of the light launched into a specific core is evenly distributed in all cores after short L. Therefore, in this discussion, we distinguish between coupling and mixing. Coupling is used to describe the degree of spatial overlap of the mode field of the core, and the degree of coupling between any two cores is measured by the mode coupling coefficient (κ), which can be calculated as follows [36]:

$$\kappa_{mn} = \frac{\omega\varepsilon_0 \int_{-\infty}^{+\infty}\int_{-\infty}^{+\infty} \left(N^2 - N_n^2\right) \boldsymbol{E}_m^* \cdot \boldsymbol{E}_n \mathrm{d}x\mathrm{d}y}{\int_{-\infty}^{+\infty}\int_{-\infty}^{+\infty} \boldsymbol{u}_z \cdot \left(\boldsymbol{E}_m^* \times \boldsymbol{H}_m + \boldsymbol{E}_m \times \boldsymbol{H}_m^*\right) \mathrm{d}x\mathrm{d}y}, \tag{2}$$

where ω is the angular frequency of the electromagnetic wave, ε_0 is the dielectric constant of the medium, $\boldsymbol{u}_z$ is the unit vector of the propagation direction $\boldsymbol{z}$, $\boldsymbol{E}_m$ and $\boldsymbol{E}_n$ represent the electric field distribution of the core m and core n in the range of the core m, respectively, and the asterisk indicates the conjugate.

Mixing describes the transfer of power between cores. The degree of mixing is measured by the power-coupling coefficient (h) based on the exponential autocorrelation function, which is calculated as follows [37, 38]:

$$h_{mn}(z) = \frac{2\kappa_{mn}^2 d}{1 + \left(\Delta\beta'_{mn} d\right)^2}, \tag{3}$$

where κ_{mn} represents the mode coupling coefficients of cores m and n, $\Delta\beta'_{mn}$ is the difference between the equivalent propagation constants of cores m and n, and d represents the correlation length, which is considered 0.05 m according to the results in [37, 38]. XT is calculated as $\text{XT} = \tanh(\bar{h} \cdot L)$, where $\bar{h}$ represents the average value of h in a period. $\bar{h}$ is positively related to XT, and thus, the described mixing is of the same nature as XT, just as a different value of XT was used in [39] to distinguish the impulse response intensity of 2-core RC-MCFs. Consider a 2-core system coupled MCF with large κ as an example; when light is launched into one of the cores to excite its local mode, it can be observed that, due to the strong coupling of the core modes, as L increases, the power of light is transferred sinusoidally to the local mode of the other core. However, when we consider this behavior from a supermode perspective, the light is launched into two first- and second-order eigen supermodes, and the observed power sinusoidal transfer between the cores is the beat frequency between the eigen supermodes that have failed to mix owing to a mismatch in propagation constants.

We consider a core number of 12 as an example to discuss the core arrangements, which is also the largest number of cores for the RC-MCF reported to date [33]. Several arrangement structures and their mode field distribution calculated by the finite element method are shown in Figure 3, corresponding to Figure 3(a) for the single-layer arrangement (SLA) and Figures 3(b)–(d) with double-layer arrangements

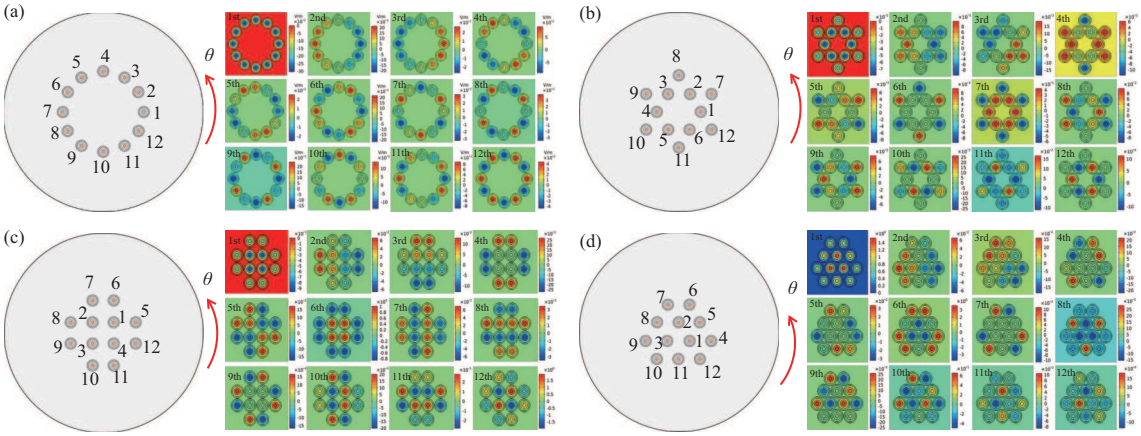

Figure 3 Schematic of core arrangement and its mode field distribution at $\theta = 0$. (a) SLA with ring structure, (b) DLA with hexagon structure, (c) DLA with square structure, and (d) DLA with triangle structure.

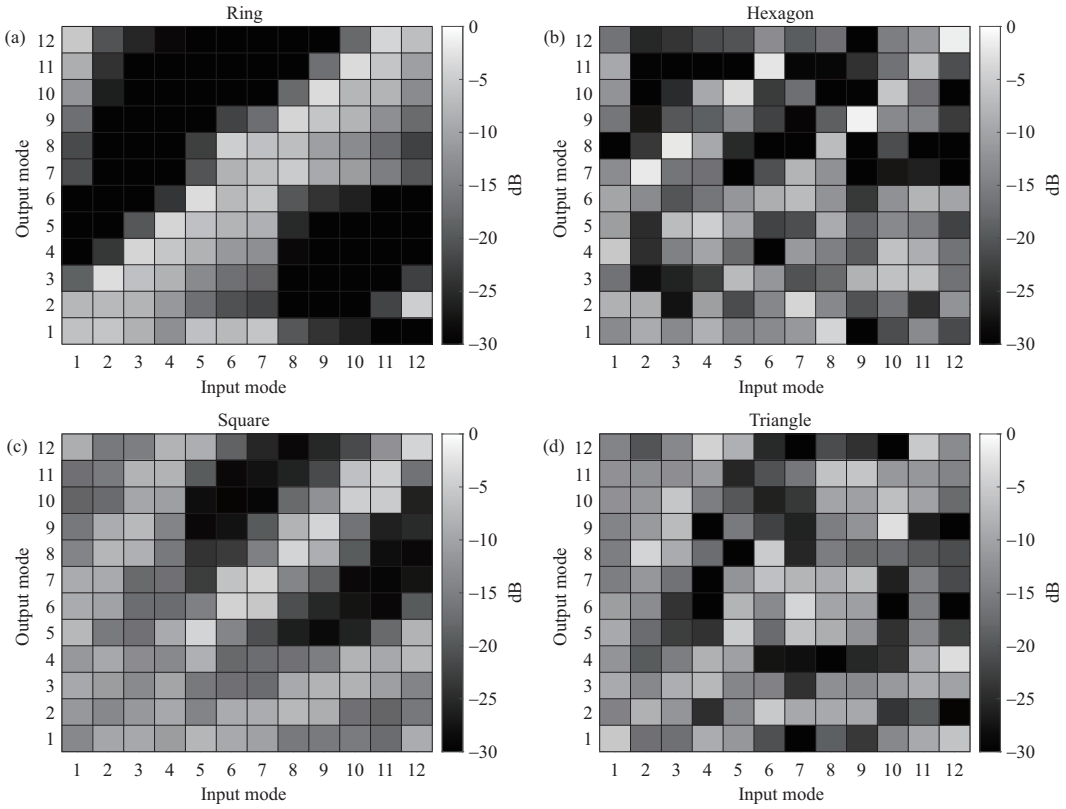

Figure 4 Mixing matrix of power under different arrangements. (a) SLA with ring structure, (b) DLA with hexagon structure, (c) DLA with square structure, and (d) DLA with triangle structure.

(DLAs), where each core structure is shown in Figure 1, $r_1 = 4.5$ μm, $a = r_1/2$, $\Delta_1 = 0.35\%$, $\Delta_2 = \Delta_1/2$, $\Delta_{\rm tr} = -0.7\%$, $r_2/r_1 = 1.5$, $W/r_1 = 0.38$, $\Lambda = 20$ μm, and $\lambda = 1550$ nm. To compare the degree of mixing, we use the beam propagation method (BPM) in the Rsoft software to simulate and calculate the power transmission process of the 12-core RC-TA-MCFs. Referring to the experimental method in [40], we excite one of the cores at the input end of the RC-TA-MCF under bending and twisting conditions, and then observe the power distribution at the output end after the fiber is twisted by π rad. Due to the mixing caused by perturbations such as bending and twisting in the RC-TA-MCF [15, 41], the mixing matrices of power shown in Figure 4 can be obtained, where $R_{\rm b} = 140$ mm, the twist rate $\gamma = 4\pi$ rad/m, $r_1 = 4.5$ μm, $a = r_1/2$, $\Delta_1 = 0.35\%$, $\Delta_2 = \Delta_1/2$, $\Delta_{\rm tr} = -0.7\%$, $r_2/r_1 = 1.5$, $W/r_1 = 0.38$, $\Lambda = 20$ μm, and $\lambda = 1550$ nm. As shown in Figure 4(a), the degree of mixing from the excited core power to the

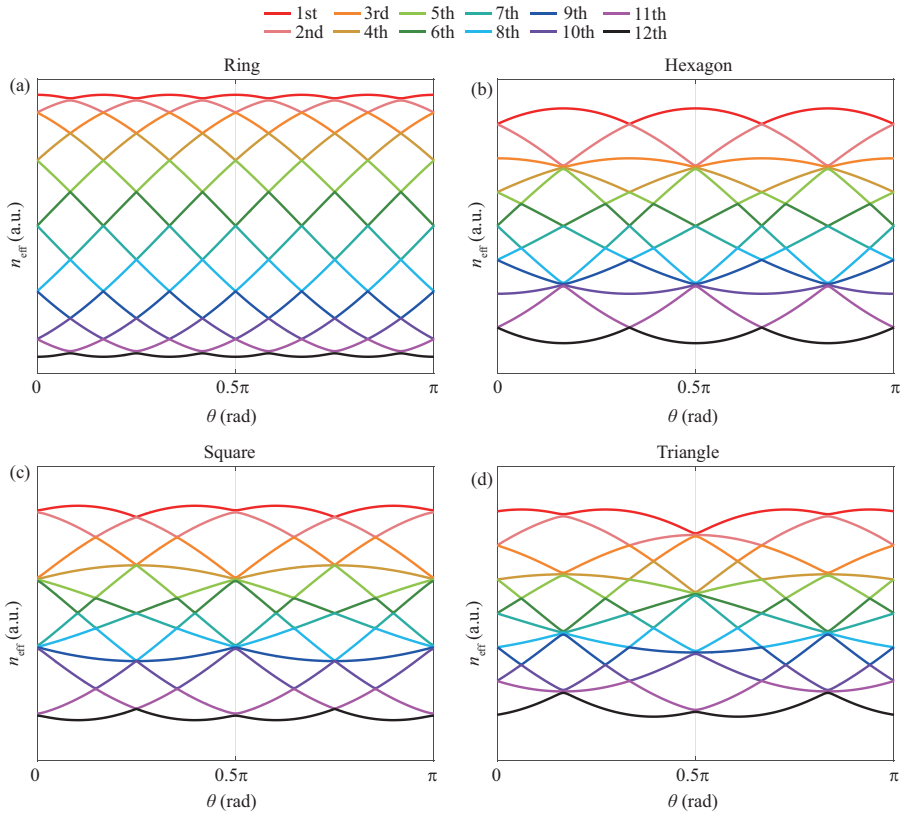

Figure 5 Dependence of n_{eff} of supermode on twisting under bending. (a) SLA with ring structure, (b) DLA with hexagon structure, (c) DLA with square structure, and (d) DLA with triangle structure.

other cores for the SLA is relatively low, while in Figures 4(b)–(d) of the DLAs, good power distributions are obtained, and thus, we can predict that the arrangement with this intermediate layer structure can achieve lower GDS characteristics under the same parameters. It should be noted that the difference among the DLAs is not obvious. Simultaneously, due to the existence of the trench layer, the degree of mixing is suppressed, and thus Λ can be reduced to improve the degree of mixing while keeping other parameters unchanged. Therefore, an RC-MCF with a low index trench can achieve a higher core density.

To further understand the reason that RC-TA-MCFs with different arrangements have different mixing properties, we calculated the dependence of n_{eff} of the corresponding supermodes on the twisting angle (θ) under the same parameters as in Figure 4, and the results are shown in Figure 5. In the SLA, the maximum n_{eff} difference (max-Δn_{eff}) between the lowest-order and highest-order supermode is larger (here, the first-order, second-order, etc. are named in descending order of supermode n_{eff}), and the variation range of n_{eff} of each supermode is small, which results in a low degree of mixing among the supermodes when propagating along the fiber. In the three different DLAs, we can observe the slight difference in max-Δn_{eff}; the max-Δn_{eff} from the largest to the smallest order is hexagon, square, and triangle.

3 GDS characteristics of RC-TA-MCF

The coupled-wave theory (CWT) [42] considers the field amplitude and phase variations and can be used to estimate random mode mixing in RC-TA-MCFs, which is essential for dealing with the variation in GDS caused by disturbances. We estimate the GDS of the 12-core RC-TA-MCFs using the CWT method described in [43, 44]. We divide the fiber of length of L into M segments, with each segment of length (ΔL) 1 mm [35, 41]. In each segment, if ΔL is small enough, the structure is assumed to be uniform. Each segment has a random twisting rate γ_z and relative to the previous segment j, there is a random twisting angle $\Delta\theta_{j+1}$ in segment $j+1$, i.e., $\theta_{j+1} = \theta_j + \Delta\theta_{j+1}$, where $\Delta\theta_{j+1} = \gamma_z \cdot \Delta L$ ($1 \leqslant j \leqslant M$), as shown in Figure 6(a).

Sufficiently random mixing among the supermodes is induced by perturbations, such as bending and

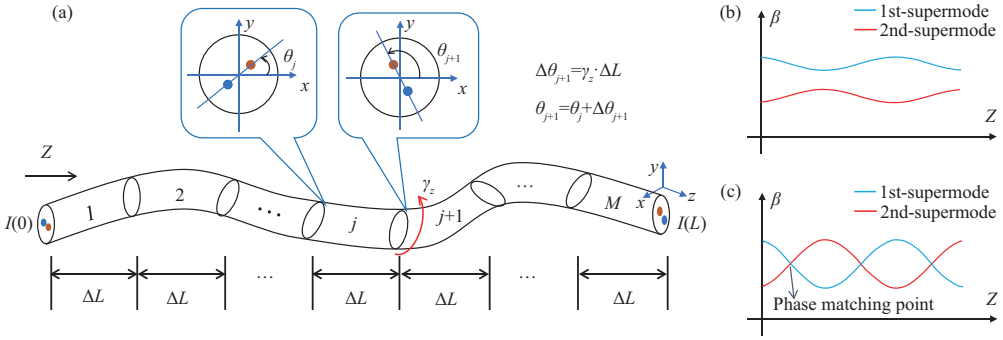

Figure 6 (Color online) Schematic of the perturbation. (a) $\Delta\theta$ applied in each segment, (b) weakly mixed, and (c) strongly mixed.

twisting. Figure 6(b) is a schematic of the perturbation, in which the variation in the propagation constant caused by bending and twisting is smaller than the difference between the propagation constants for different modes, and the corresponding modes are not sufficiently mixed and are in a weakly mixed state. In contrast, Figure 6(c) shows a schematic showing that bending and twisting induce sufficient mixing and lead to a strongly mixed state. Similar to the method of using a twisting device to reduce the polarization mode dispersion (PMD) in single-mode fibers [45], sinusoidally modulated bidirectional twisting is used to simulate the twisting device in the drawing process of RC-TA-MCF [46], and the peak rate of twisting (T_p) is 1, 3, or 5 turns/m. Simultaneously, a Gaussian random quantity with mean value of 0 and standard deviation of σ turns/m is introduced in the twisting process to simulate the random fluctuation in the real fiber; a similar simulation has been applied in [47]. Owing to the introduction of random quantities in the calculation of GDS, the calculation results of GDS presented here are the average values of 30 iterations. The initial state $\boldsymbol{I}(0)_{N\times N}$ of each mode in the RC-TA-MCF is transformed by a transmission matrix $\boldsymbol{T}(\omega)_{N\times N}$, and the state becomes $\boldsymbol{I}(L)_{N\times N}$ when transferred to the L, that is, $\boldsymbol{I}(L) = \boldsymbol{T}(\omega)\cdot\boldsymbol{I}(0)$. Therefore, the group delay operator GDO is defined by $\boldsymbol{T}(\omega)$ as [43, 44]

$$\mathrm{GDO}(\omega) = j\cdot\boldsymbol{T}(\omega)^{-1}\cdot\frac{\mathrm{d}\boldsymbol{T}(\omega)}{\mathrm{d}\omega}. \tag{4}$$

The calculation formula of GDS can be obtained from the GDO operator as follows:

$$\mathrm{GDS} = \sqrt{\frac{1}{N}\sum_{i=1}^{N}\tau_i^2}, \tag{5}$$

where N is the total number of modes containing polarization states and τ_i is the i-th eigenvalue of the GDO operator.

Figure 7(a) shows the results of simulating a step 4-core RC-MCF at a length of 10 km with different ΔL, where the 4 cores are arranged in a square pattern, $r_1 = 4.5$ μm, $\Delta_1 = 0.35\%$, $\Lambda = 20$ μm, $R_\mathrm{b} = 140$ mm, $T_p = 3$ turns/m, $\sigma = 0.3$ turn/m, and $\lambda = 1550$ nm. The solid line in Figure 7(a) represents the average value of 30 results, which is used to denote the value of GDS, and the error bar represents the standard deviation (SD) of the calculated GDS. It can be observed that the error bar is positively correlated with ΔL, the GDS converges when ΔL decreases to 1 mm, and the SD does not change dramatically with respect to the mean value. Therefore, in our calculations, $\Delta L = 1$ mm is used and the mean of 30 results is used to represent the GDS. To observe the influence of the manufacturing error tolerance and Λ on the TA-core under different core arrangements, the core size error is estimated as $r_1 \pm 0.1$ μm (approximately 2%). The GDS after transmission of $L = 1$ km under different Λ was calculated, and the results are shown in Figure 7(b), where r_1 is a random value in the range of 4.5 ± 0.1 μm, $a = r_1/2$, $\Delta_1 = 0.35\%$, $\Delta_2 = \Delta_1/2$, $\Delta_\mathrm{tr} = -0.7\%$, $r_2/r_1 = 1.5$, $W/r_1 = 0.38$, $\lambda = 1550$ nm, $T_p = 3$ turn/m, $\sigma = 0.3$ turn/m, and $R_\mathrm{b} = 140$ mm. As shown in Figure 7(b) for the SLA, it is difficult to achieve sufficient mixing because there is no transition of the intermediate layer, and thus, a smaller Λ is required to enhance its degree of mixing. However, the value of Λ is physically limited (that is, $\Lambda \geqslant 2r_3$), which cannot be reduced without restraint, such that the corresponding GDS value is larger in the whole range of Λ. In contrast, for the DLA, a larger degree of mixing always makes its GDS value lower than that of the SLA. We can also find that the difference among the different DLAs is small, and

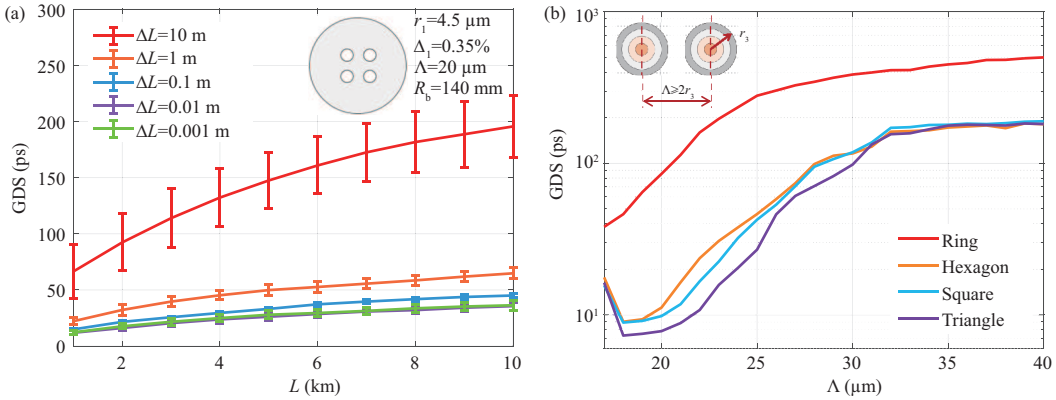

Figure 7 (a) Dependence of GDS on L for different ΔL in 4-core RC-MCF; (b) dependence of GDS on Λ after $L = 1$ km propagation in 12-core RC-MCF.

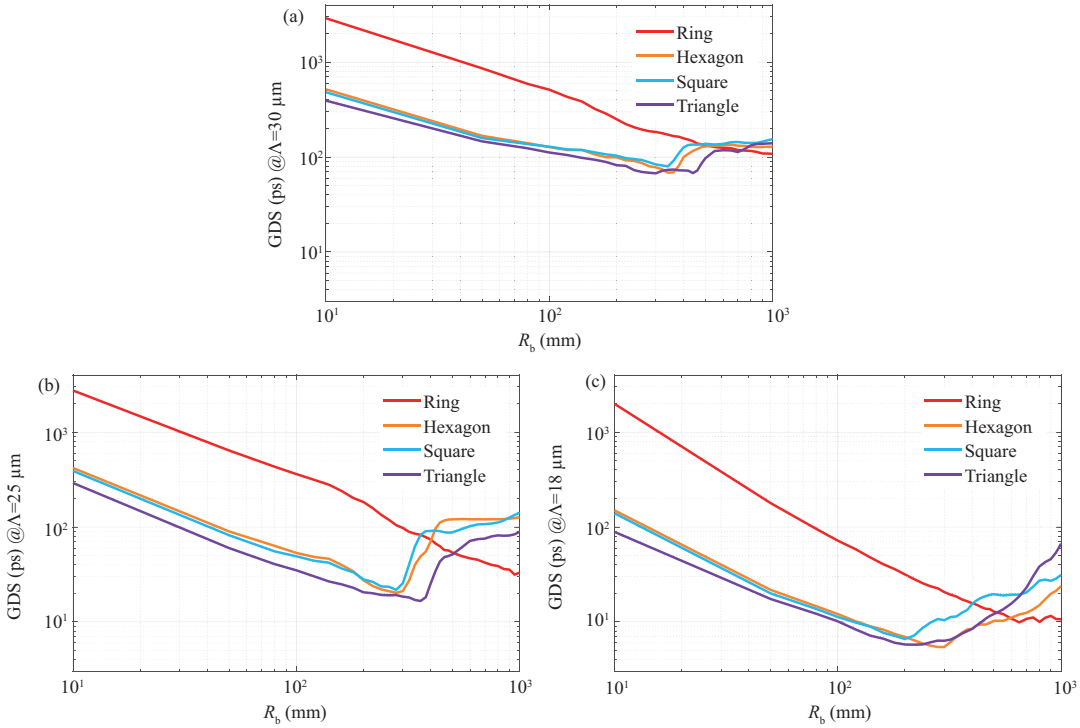

Figure 8 Dependence of GDS on R_b after 1 km propagation under different arrangements. (a) $\Lambda = 30$ μm, (b) $\Lambda = 25$ μm, and (c) $\Lambda = 18$ μm.

the minimum GDS is obtained when $\Lambda = 18$ μm. It can also be observed that when $R_\mathrm{b} = 140$ mm, the DLA with a triangle structure can obtain a smaller GDS and wider selection range of Λ; these trends are well corresponding to those in Figure 5.

Figure 8 shows the relationship between the GDS and R_b of the 12-core RC-TA-MCF with different arrangements when $\Lambda = 18$, 25, and 30 μm, respectively, where r_1 is a random value in the range of 4.5 ± 0.1 μm, $a = r_1/2$, $\Delta_1 = 0.35\%$, $\Delta_1 = \Delta_1/2$, $\Delta_\mathrm{tr} = -0.7\%$, $r_1/r_2 = 1.5$, $W/r_1 = 0.38$, $\lambda = 1550$ nm, $T_p = 3$ turn/m, $\sigma = 0.3$ turn/m, and $R_\mathrm{b} = 140$ mm. For $\Lambda = 30$ μm as shown in Figure 8(a), due to the small degree of coupling (κ), each core tends to be independent. With an increase in R_b, the modulation effect of bending and twisting on the index decreases, and the propagation constants of each core tend to be the same. Therefore, for the SLA with a large GDS, with an increase in R_b, the GDS decreases and converges to the inter-core-skew (ICS) caused by manufacturing errors. For a DLA with a small GDS, with an increase in R_b, the GDS decreases, possibly becoming smaller than the ICS. When $R_\mathrm{b} > 400$ mm, the GDS increases and gradually converges with the ICS. For the case of $\Lambda = 18$ μm as shown in Figure 8(c), the degree of coupling (κ) is larger, and the mode is confined in the core when

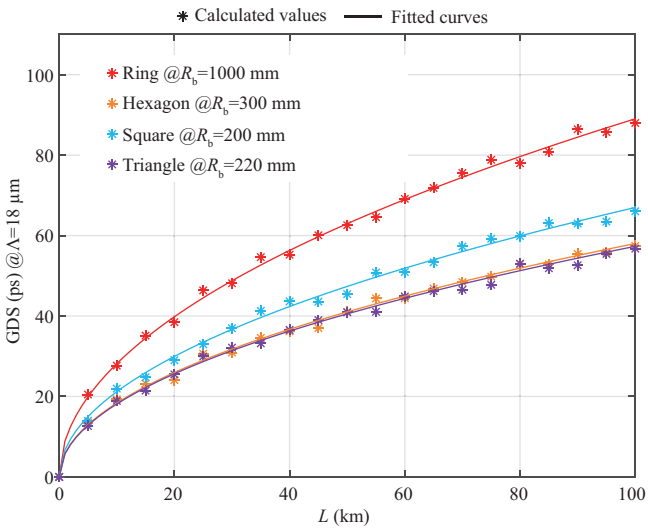

Figure 9 Dependence of GDS on L under the optimal R_b of different arrangements when $\Lambda = 18$ μm.

the R_b is small. With an increase in R_b (from 10 to 300 mm), the mode distribution gradually spreads over all the cores. Bending and twisting induce random mixing, which causes a variation of n_eff greater than Δn_eff among different supermodes, as shown in Figure 6(c), such that the GDS decreases, even to below a few pico-seconds (ps). When R_b is large enough ($\geqslant$ 400 mm), gradually stable supermodes are formed, while the large R_b is not enough to induce random mixing, as shown in Figure 6(b), such that the GDS increases with the increase of R_b and tends to lead to differential mode delay (DMD) among supermodes. The case of $\Lambda = 25$ μm, as shown in Figure 8(b), is an intermediate situation between the above two cases. Therefore, the GDS in RC-MCFs does not decrease with increasing R_b, and this relationship between R_b and GDS has been demonstrated by experimental measurements of coupled 4-core fibers [47]. The bending conditions can be further divided into tight bending conditions ($R_\mathrm{b} \leqslant 300$ mm) and weak bending conditions ($R_\mathrm{b} \geqslant 400$ mm) [48]. To better control the bending and twisting conditions of fabricated fibers in practical applications and enhance the controllability of the coefficient of spatial mode dispersion (SMD) by achieving a strongly mixed state, a bundle tape is used to exert tension on the bundled fibers [49], and the magnitude of SMD remains unchanged in the raw fiber compared with that after cabling [50]. Subsequently, we calculate the dependence of GDS on the L under the optimal R_b of different arrangements when $\Lambda = 18$ μm in Figure 8(c); the optimal R_b of SLA with ring structure is 1000 mm, that of the DLA with a hexagonal structure is 300 mm, that of the DLA with a square structure is 200 mm, and that of the DLA with a triangular structure is 220 mm. The results are shown in Figure 9, where the asterisks represent the values calculated using (4) and (5), and the solid lines represent the curves fitted to the values. The SMD coefficients for each arrangement are obtained from the fitted curves. The SMD coefficient of the SLA with ring structure is 8.904 ps/$\sqrt{\mathrm{km}}$ at $R_\mathrm{b} = 1000$ mm, that of the DLA with hexagonal structure is 5.802 ps/$\sqrt{\mathrm{km}}$ at $R_\mathrm{b} = 300$ mm, that of the DLA with square structure is 6.698 ps/$\sqrt{\mathrm{km}}$ at $R_\mathrm{b} = 200$ mm, and that of the DLA with triangular structure is 5.733 ps/$\sqrt{\mathrm{km}}$ at $R_\mathrm{b} = 220$ mm.

We also notice in Figure 8 that when R_b is small, the GDS from maximum to minimum corresponds to the SLA and the DLAs with hexagon, square, and triangle. When R_b is large or even infinite (i.e., the fiber is straight), the trend is reversed. To explain the reason for this trend, the n_eff of each order supermode under different arrangements is calculated, and the results are shown in Figure 10; Figure 10(a) has R_b =140 mm and $\theta = 0$ rad, and Figure 10(b) has straight and $\theta = 0$ rad. As shown in Figure 10, the variation trend of max-Δn_eff between different arrangements from bending to straight corresponds exactly to that of GDS. Furthermore, for the DLAs, bending can change not only the max-Δn_eff but also the degeneracy among supermodes, such that random mixing among different modes is sufficient when propagating along the fiber. For the SLA, bending only changes max-Δn_eff, not the degeneracy among modes. Therefore, to design an RC-MCF, the DLA can be considered, which can enable sufficient coupling and mixing among different supermodes under perturbations such as bending and twisting. To design a systematically coupled MCF similar to the few-mode fiber [13,14], the SLA can be considered. As the fiber propagates, longitudinal disturbances will cause mixing among supermodes, which should be

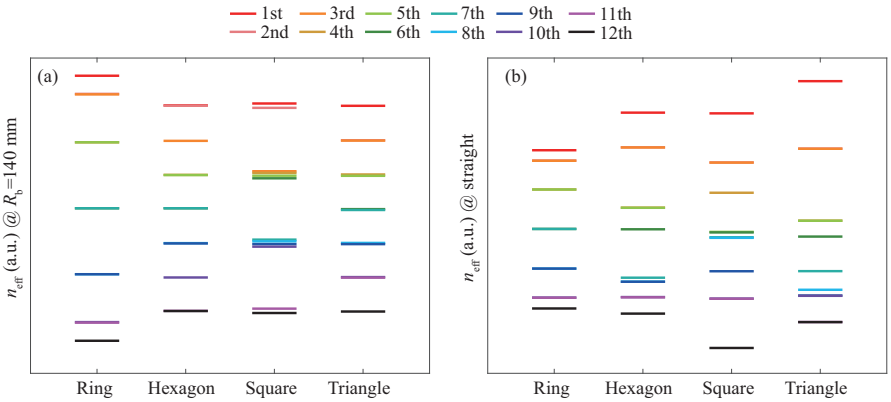

Figure 10 n_{eff} of supermodes with different arrangements when $\Lambda = 18$ μm. (a) $R_{\mathrm{b}} = 140$ mm and (b) straight ($R_{\mathrm{b}} \to +\infty$).

avoided for the systematically coupled MCF. However, this mixing can be suppressed by increasing the mismatch of propagation constants; in other words, we can reduce Λ to further increase the propagation constant difference among different supermodes.

4 Conclusion

We first studied a type of inner-depressed TA-core that can be used as a subcomponent of an RC-MCF. For maintaining the single-mode condition as well as large A_{eff} (larger than 82 μm^2 of the conventional SMF), the parameters of the inner core are set as $a = r_1/2$ and $\Delta_2 = \Delta_1/2$. By changing the corresponding parameters of trench (e.g., r_2, W, Δ_{tr}), the ΔNg of the core can be adjusted to be as close as possible to 0, to enhance the tolerance of manufacturing errors.

The designed core is then applied to RC-MCFs with different arrangements to study the dependence of the degree of mixing on bending and twisting. It is found that a low-index trench layer allows strong mixing with smaller Λ, and thus the core density can be enhanced while keeping other parameters of the core structure unchanged. For the core arrangement type of SLA, it is difficult to achieve a higher degree of mixing within the allowable range due to the physical limitation of the minimum Λ (as $\Lambda \geqslant 2r_3$ is required). For the core arrangement type of DLA, if the parameters of the core structure and the bending conditions of the waveguide are fixed, there is a moderate Λ (approximately 18–21 μm) to reduce GDS; i.e., there is a trade-off relationship between low GDS and small Λ. Similarly, if the parameters of the core structure and Λ are fixed, there is a moderate R_{b} (approximately 100–400 mm, i.e., the transition area of the tight and weak bending conditions) to reduce GDS; thus, R_{b} can be moderately increased to reduce GDS. However, to minimize the GDS and keep the SMD coefficient below 10 ps/$\sqrt{\mathrm{km}}$, it is necessary to choose a region with "strongly coupled, strongly mixed", which is determined by Λ and R_{b} when the parameters of the core structure are fixed. Conversely, compared with the SLA, all DLAs can obtain a small GDS and the difference among them is not obvious.

Therefore, a DLA with a high degree of mixing is suitable for realizing an RC-MCF, which has a higher spatial density and lower GDS, while an SLA with a low degree of mixing can be a good candidate for systematically coupled MCFs, similar to the few-mode fiber used in mode-division multiplexing transmission systems.

Acknowledgements This work was supported by National Key Research and Development Program of China (Grant No. 2021YFB2800901), National Natural Science Foundation of China (Grant Nos. U2001601, 62035018), Guangzhou Basic and Applied Basic Research Foundation (Grant No. 202002030327), and Guangdong Basic and Applied Basic Research Foundation (Grant No. 2023A1515012984).

References

1 Morioka T, Awaji Y, Ryf R, et al. Enhancing optical communications with brand new fibers. IEEE Commun Mag, 2012, 50: 31–42
2 Winzer P J, Neilson D T, Chraplyvy A R. Fiber-optic transmission and networking: the previous 20 and the next 20 years. Opt Express, 2018, 26: 24190–24239
3 Essiambre R J, Kramer G, Winzer P J, et al. Capacity limits of optical fiber networks. J Lightwave Technol, 2010, 28: 662–701

4 Hamaoka F, Minoguchi K, Sasai T, et al. 150.3-Tb/s ultra-wideband (S, C, and L bands) single-mode fiber transmission over 40-km using > 519 Gb/s/A PDM-128QAM signals. In: Proceedings of the 44th European Conference on Optical Communication (ECOC 2018), Roma, 2018. 1–3
5 Saitoh K, Matsuo S. Multicore fiber technology. J Lightwave Technol, 2016, 34: 55–66
6 Li M J, Hayashi T. Advances in low-loss, large-area, and multicore fibers. In: Proceedings of Optical Fiber Telecommunications VII, 2020. 3–50
7 Hayashi T. Design of multi-core and coupled-core fibers. In: Proceedings of IEEE Photonics Society Summer Topical Meeting Series, Hawaii, 2018. 173–174
8 Saitoh K. Multi-core fiber technology for SDM: coupling mechanisms and design. J Lightwave Technol, 2022, 40: 1527–1543
9 Saitoh K, Matsuo S. Multicore fibers for large capacity transmission. Nanophotonics, 2013, 2: 441–454
10 Matsui T, Pondillo P L, Nakajima K. Weakly coupled multicore fiber technology, deployment, and systems. Proc IEEE, 2022, 110: 1772–1785
11 Sakamoto T, Mori T, Wada M, et al. Strongly-coupled multi-core fiber and its optical characteristics for MIMO transmission systems. Optical Fiber Tech, 2017, 35: 8–18
12 Sakamoto T, Mori T, Wada M, et al. Coupled single-mode multi-core fiber design for long-haul MIMO transmission system. In: Proceedings of Optical Fiber Communication Conference, Los Angeles, 2017
13 Xia C, Bai N, Ozdur I, et al. Supermodes for optical transmission. Opt Express, 2011, 19: 16653–16664
14 Xia C, Bai N, Amezcua-Correa R, et al. Supermodes in strongly-coupled multi-core fibers. In: Proceedings of Optical Fiber Communication Conference and Exposition and the National Fiber Optic Engineers Conference, Anaheim, 2013. 1–3
15 Sakamoto T, Mori T, Wada M, et al. Fiber twisting- and bending-induced adiabatic/nonadiabatic super-mode transition in coupled multicore fiber. J Lightwave Technol, 2016, 34: 1228–1237
16 Huang B, Fontaine N K, Chen H, et al. Minimizing the modal delay spread in coupled-core two-core fiber. In: Proceedings of Conference on Lasers and Electro-Optics (CLEO 2016), San Jose, 2016. 1–2
17 Matsuo S, Sasaki Y, Ishida I, et al. Recent progress on multi-core fiber and few-mode fiber. In: Proceedings of Optical Fiber Communication Conference, Anaheim, 2013
18 Sillard P. Few-mode fibers for space division multiplexing. In: Proceedings of Optical Fiber Communication Conference, Optica Publishing Group, Anaheim, 2016
19 Rademacher G, Puttnam B J, Luís R S, et al. 10.66 peta-bit/s transmission over a 38-core-three-mode fiber. In: Proceedings of Optical Fiber Communication Conference, San Diego, 2020
20 Sakamoto T, Saitoh K, Saitoh S, et al. 120 spatial channel few-mode multi-core fiber with relative core multiplicity factor exceeding 100. In: Proceedings of the 44th European Conference on Optical Communication (ECOC 2018), Roma, 2018. 1–3
21 Hayashi T, Sakamoto T, Yamada Y, et al. Randomly-coupled multi-core fiber technology. Proc IEEE, 2022, 110: 1786–1803
22 Hayashi T, Ryf R, Fontaine N K, et al. Coupled-core multi-core fibers: high-spatial-density optical transmission fibers with low differential modal properties. In: Proceedings of European Conference on Optical Communication, Valencia, 2015. 1–3
23 Ho K P, Kahn J M. Statistics of group delays in multimode fiber with strong mode coupling. J Lightwave Technol, 2011, 29: 3119–3128
24 Ho K P, Kahn J M. Linear propagation effects in mode-division multiplexing systems. J Lightwave Technol, 2014, 32: 614–628
25 Antonelli C, Mecozzi A, Shtaif M, et al. Stokes-space analysis of modal dispersion in fibers with multiple mode transmission. Opt Express, 2012, 20: 11718–11733
26 van der Heide S, Alvarado-Zacarias J C, Fontaine N K, et al. Low-loss low-MDL core multiplexer for 3-core coupled-core multi-core fiber. In: Proceedings of Optical Fiber Communications Conference and Exhibition, San Diego, 2020. 1–3
27 Antonelli C, Mecozzi A, Shtaif M, et al. Stokes-space analysis of modal dispersion of SDM fibers with mode-dependent loss: theory and experiments. J Lightwave Technol, 2019, 38: 1668–1677
28 Ho K P. Exact model for mode-dependent gains and losses in multimode fiber. J Lightwave Technol, 2012, 30: 3603–3609
29 Agrawal G P, Essiambre R J. Nonlinear limits of SDM transmission. In: Proceedings of IEEE Photonics Society Summer Topical Meeting Series, Montreal, 2014. 174–175
30 Antonelli C, Golani O, Shtaif M, et al. Nonlinear interference noise in space-division multiplexed transmission through optical fibers. Opt Express, 2017, 25: 13055–13078
31 Ryf R, Alvarado-Zacarias J C, Wittek S, et al. Coupled-core transmission over 7-core fiber. In: Proceedings of Optical Fiber Communication Conference, San Diego, 2019
32 Saitoh K, Fujisawa T, Sato T. Coiling size dependence of group delay spread in coupled multicore fibers without intentional twisting. J Lightwave Technol, 2017, 35: 4559–4566
33 Sakamoto T, Aozasa S, Mori T, et al. Randomly-coupled single-mode 12-core fiber with highest core density. In: Proceedings of Optical Fiber Communications Conference and Exhibition, San Francisco, 2017. 1–3
34 Sakamoto T, Mori T, Wada M, et al. Coupled multicore fiber design with low intercore differential mode delay for high-density space division multiplexing. J Lightwave Technol, 2015, 33: 1175–1181
35 Saitoh K, Fujisawa T, Sato T. Control of group delay spread in randomly-coupled multicore fibers. In: Proceedings of Opto-Electronics and Communications Conference, San Diego, 2020. 1–3
36 Tu J, Saitoh K, Koshiba M, et al. Optimized design method for bend-insensitive heterogeneous trench-assisted multi-core fiber with ultra-low crosstalk and high core density. J Lightwave Technol, 2013, 31: 2590–2598
37 Koshiba M, Saitoh K, Takenaga K, et al. Multi-core fiber design and analysis: coupled-mode theory and coupled-power theory. Opt Express, 2011, 19: 102–111
38 Koshiba M, Saitoh K, Takenaga K, et al. Analytical expression of average power-coupling coefficients for estimating intercore crosstalk in multicore fibers. IEEE Photonics J, 2012, 4: 1987–1995
39 Puttnam B J, Rademacher G, Luís R S. Space-division multiplexing for optical fiber communications. Optica, 2021, 8: 1186–1203
40 Ryf R, Essiambre R J, Randel S, et al. Impulse response analysis of coupled-core 3-core fibers. In: Proceedings of the 38th European Conference and Exhibition on Optical Communications, Amsterdam, 2012. 1–3
41 Sakamoto T, Mori T, Wada M, et al. Fiber twisting and bending induced mode conversion characteristics in coupled multi-core fiber. In: Proceedings of European Conference on Optical Communication, Valencia, 2015. 1–3
42 Haus H A, Molter-Orr L. Coupled multiple waveguide systems. IEEE J Quantum Electron, 1983, 19: 840–844
43 Fujisawa T, Saitoh K. Group delay spread analysis of strongly coupled 3-core fibers: an effect of bending and twisting. Opt Express, 2016, 24: 9583–9591
44 Fujisawa T, Saitoh K. Group delay spread analysis of coupled-multicore fibers: a comparison between weak and tight bending

conditions. Optics Commun, 2017, 393: 232–237
45 Mohanty S, Sridhar N, Sinha S, et al. Method for producing twisted optical fiber with reduced polarization mode dispersion. United States patent US 7,310,974. 2007-12-25
46 Chen X, Li M J, Heron N A, et al. Method of imparting twist to optical fiber. United States. Patent US 7,317,855. 2008-1-8
47 Hayashi T, Tamura Y, Hasegawa T, et al. Record-low spatial mode dispersion and ultra-low loss coupled multi-core fiber for ultra-long-haul transmission. J Lightwave Technol, 2017, 35: 450–457
48 Saitoh K, Fujisawa T, Sato T. Design and analysis of weakly-and strongly-coupled multicore fibers. In: Proceedings of Photonic Networks and Devices, New Orleans, 2017
49 Yamada Y, Sakamoto T, Wada M, et al. Design of high-density cable parameters for controlling spatial-mode dispersion of randomly coupled multi-core fibers. J Lightwave Technol, 2021, 39: 1179–1185
50 Arikawa M, Wu M, Yasuhara K, et al. Long-haul WDM/SDM transmission over coupled 4-core fibers installed in submarine cable. J Lightwave Technol, 2023, 41: 1649–1657